# Immunity

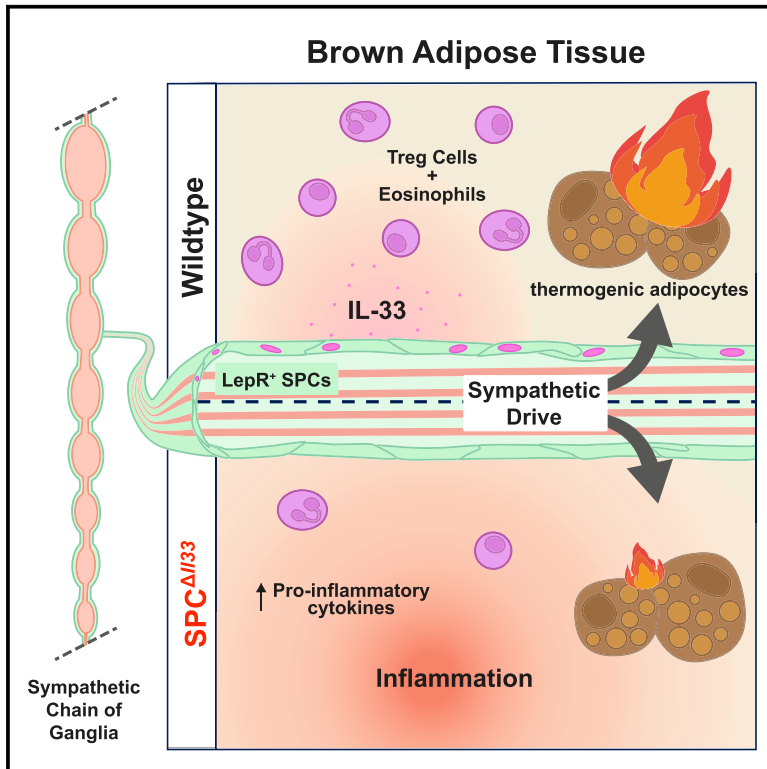# Immunomodulatory leptin receptor⁺ sympathetic perineurial barrier cells protect against obesity by facilitating brown adipose tissue thermogenesis

## Graphical abstract



## Authors

Emma R. Haberman, Gitalee Sarker, Bernardo A. Arús, ..., Miguel López, Florent Ginhoux, Ana I. Domingos

## Correspondence

ana.domingos@dpag.ox.ac.uk

## In brief

Chronic, low-grade inflammation, dysregulation of leptin signaling and reduced sympathetic drive underlie adipose tissue dysfunction in obesity, although links between these causes are presently unclear. Haberman et al. identify a population of LepR+ sympathetic perineurial barrier cells that ensheathe bundles of nerves and facilitate adaptive thermogenesis by preventing inflammation.

## Highlights

- Sympathetic perineurial barrier cells (SPCs) express LepR and IL-33 in mice and humans

- SPC-derived IL-33 prevents BAT inflammation via Treg cell and eosinophil recruitment

- Adaptive thermogenesis is impaired in SPC$^{\Delta Il33}$ mice

- LepR⁺ SPCs link leptin to immunometabolic regulation of body weight homeostasis

CellPress

# Immunity

**CellPress**

## Article

# Immunomodulatory leptin receptor+ sympathetic perineurial barrier cells protect against obesity by facilitating brown adipose tissue thermogenesis

Emma R. Haberman,[1] Gitalee Sarker,[1] Bernardo A. Arús,[2,3] Karin A. Ziegler,[4,5] Sandro Meunier,[4,5]
Noelia Martínez-Sánchez,[1,2] Eliška Freibergerová,[1] Sinem Yilmaz-Özcan,[2] Iara Fernández-González,[6] Chloe Zentai,[1]
Conan J.O. O'Brien,[1] David E. Grainger,[7] Davi Sidarta-Oliveira,[1] Svetoslav Chakarov,[8,9] Andrea Raimondi,[10]
Matteo Iannacone,[10,11] Stefan Engelhardt,[4,5] Miguel López,[6] Florent Ginhoux,[8,9] and Ana I. Domingos[1,12,*]

[1]Department of Physiology, Anatomy and Genetics, University of Oxford, Oxford, UK
[2]Instituto Gulbenkian de Ciência, Oeiras, Portugal
[3]Helmholtz-Zentrum Dresden – Rossendorf (HZDR), Dresden, Germany
[4]Institute of Pharmacology and Toxicology, Technical University Munich (TUM), Munich, Germany
[5]DZHK (German Centre for Cardiovascular Research), Partner Site Munich Heart Alliance, Munich, Germany
[6]Neurobesity Group, Department of Physiology, Center for Research in Molecular Medicine and Chronic Diseases (CiMUS), Universidade de Santiago de Compostela, Santiago, Spain
[7]Weatherall Institute of Molecular Medicine, University of Oxford, Oxford, UK
[8]Singapore Immunology Network (SIgN), A*STAR, Singapore, Singapore
[9]Shanghai Institute of Immunology, Department of Immunology and Microbiology, Shanghai Jiao Tong University School of Medicine, Shanghai 200025, China
[10]Vita-Salute San Raffaele University, Milan, Italy
[11]Division of Immunology, Transplantation and Infectious Diseases, IRCCS San Raffaele Scientific Institute, Milan, Italy
[12]Lead contact
*Correspondence: ana.domingos@dpag.ox.ac.uk
https://doi.org/10.1016/j.immuni.2023.11.006

## SUMMARY

Adipose tissues (ATs) are innervated by sympathetic nerves, which drive reduction of fat mass via lipolysis and thermogenesis. Here, we report a population of immunomodulatory leptin receptor-positive (LepR+) sympathetic perineurial barrier cells (SPCs) present in mice and humans, which uniquely co-express *Lepr* and interleukin-33 (*Il33*) and ensheath AT sympathetic axon bundles. Brown ATs (BATs) of mice lacking IL-33 in SPCs (SPC^ΔIl33) had fewer regulatory T (Treg) cells and eosinophils, resulting in increased BAT inflammation. SPC^ΔIl33 mice were more susceptible to diet-induced obesity, independently of food intake. Furthermore, SPC^ΔIl33 mice had impaired adaptive thermogenesis and were unresponsive to leptin-induced rescue of metabolic adaptation. We therefore identify LepR+ SPCs as a source of IL-33, which orchestrate an anti-inflammatory BAT environment, preserving sympathetic-mediated thermogenesis and body weight homeostasis. LepR+IL-33+ SPCs provide a cellular link between leptin and immune regulation of body weight, unifying neuroendocrinology and immunometabolism as previously disconnected fields of obesity research.

## INTRODUCTION

Adipose tissue (AT)-resident immune cells have been extensively implicated in obesity, which is linked with chronic, low-grade inflammation of the AT.[1] This is reflected in an increase of pro-inflammatory AT macrophages and a concomitant reduction in anti-inflammatory immune cells, including regulatory T (Treg) cells and eosinophils.[2–8] In tandem with immunometabolic regulation, body weight is chiefly controlled by the hormone leptin. Leptin is released from ATs proportional to fat mass where it acts on hypothalamic leptin receptor-positive (LepR+) neurons to increase downstream sympathetic drive onto ATs, stimulating thermogenesis in brown AT (BAT).[1,9–11] This neuroendocrine loop of leptin action is disrupted in obesity, where sympathetic

drive onto ATs is suppressed and downstream BAT thermogenesis is blunted, further worsening weight gain.[12] Studies on the neuroendocrine and immune regulation of ATs have been separated, with no biological players linking the two fields.[13] Here, we identify one such cellular intermediate, providing a missing link bridging the neuroendocrine loop of leptin action with immune regulation of energy homeostasis.

## RESULTS

### A LepR+ SPC barrier ensheathes sympathetic ganglia and AT axon bundles

Sympathetic neurons innervate ATs via the paravertebral sympathetic ganglia (Figure 1A). Considering the role of leptin in AT
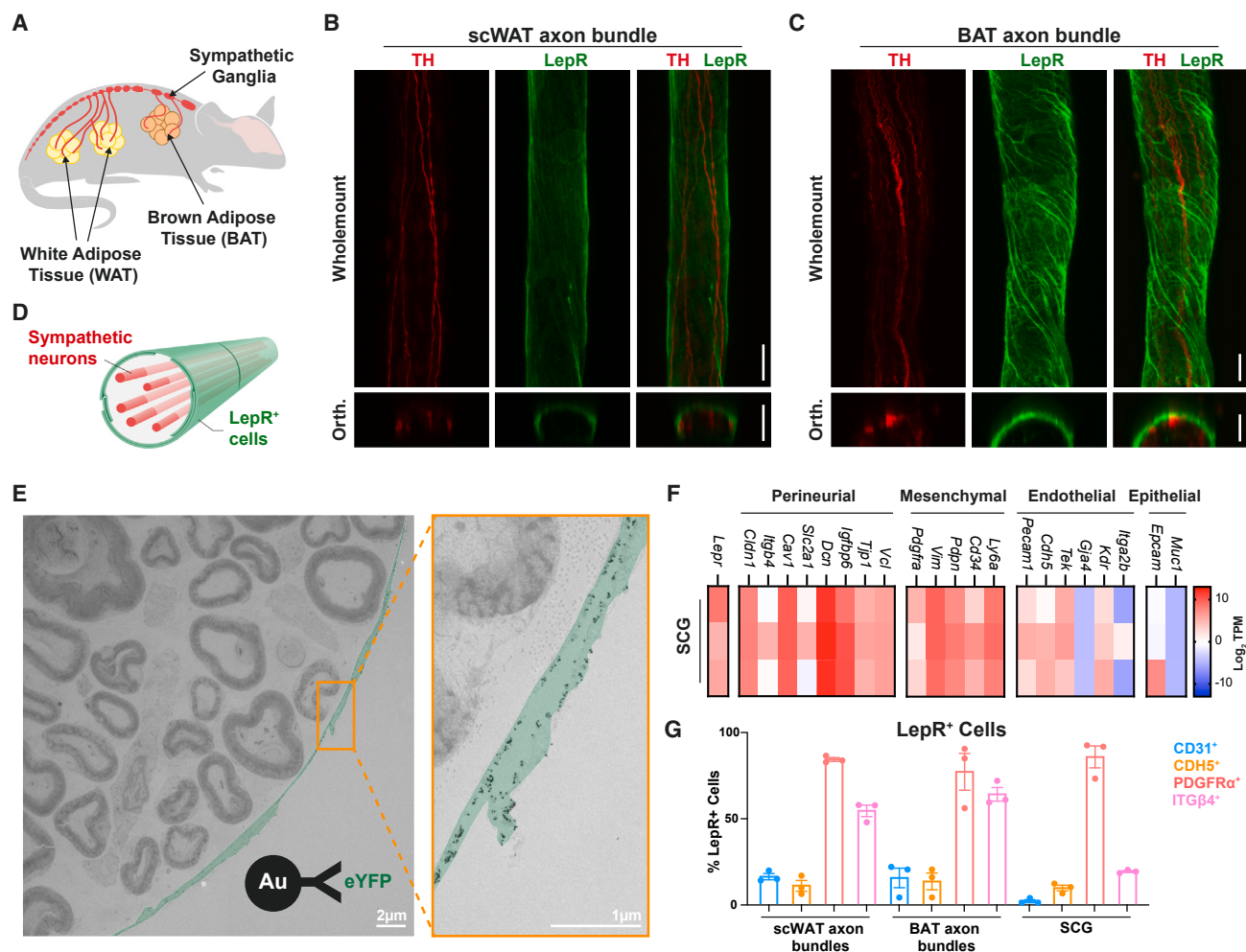
**Figure 1. A LepR+ sympathetic perineurial cell (SPC) barrier ensheathes sympathetic ganglia and adipose tissue axon bundles**

(A) Schematic representation: adipose tissue is innervated by sympathetic axon bundles originating from the paravertebral chain of sympathetic ganglia.[10,17,18]

(B and C) Sympathetic axon bundles dissected from the subcutaneous white adipose tissue (scWAT, B) or brown adipose tissue (BAT, C) are surrounded by a LepR+ cell barrier. LepR^eYFP mice, 20× maximum intensity projection images (whole mount) or orthogonal optical reconstruction (Orth). TH, tyrosine hydroxylase (red); LepR^eYFP (green). Scale bars, 25 μm.

(D) Schematic representation: sympathetic neurons are surrounded by a LepR+ barrier in adipose tissue nerves.

(E) Transmission electron micrograph of a scWAT sympathetic axon bundle cross section. Immuno-EM staining with dense, gold-conjugated anti-eYFP antibodies reveals a multi-layer LepR+ perineurial cell barrier. scWAT fiber dissected from LepR^eYFP mice. LepR cells false-colored in green. Scale bars, 2 μm.

(F) Bulk RNA-seq of LepR+ cells sorted from the superior cervical ganglia (SCG) of LepR^eYFP mice (n = 3). LepR+ cells express Lepr and highly express perineurial and mesenchymal cell markers. Data presented as $\log_2$ transcripts per million (TPM).

(G) Flow cytometric analysis of LepR+ cells isolated from sympathetic tissues (scWAT axon bundles, BAT axon bundles, and SCG). LepR+ sympathetic perineurial cells (SPCs in sympathetic tissues are PDGFRα+ITGβ4+). LepR^eYFP mice (n = 3). Full gating strategy in Figure S1B. Data presented as mean ± SEM.

See also Figure S1.

lipolysis and thermogenesis,[10] we investigated the presence of LepR+ cells within AT sympathetic axon bundles. Immunofluorescence (IF) imaging of sympathetic tissues dissected from LepR^eYFP mice—where expression of LepR results in the expression of enhanced yellow fluorescent protein (eYFP)—revealed a LepR+ cell barrier ensheathing both subcutaneous white AT (scWAT) and BAT axon bundles (Figures 1B–1D; Videos S1 and S2), as well as sympathetic ganglia (Figure S1A). Using IF imaging, we confirmed that the observed LepR^eYFP fluorescence was not found in AT neurons, co-staining for pan-neuronal marker B3-TUB (Figure S1B; Videos S1 and S2). We detected

similar frequencies of LepR+ cells in all sympathetic tissues (Figures S1C and S1D). To visualize the ultrastructure of this LepR+ cell barrier, we performed immuno-electron microscopy (immuno-EM) on cross sections of LepR^eYFP scWAT axon bundles, using dense, gold-conjugated anti-eYFP antibodies to mark LepR+ cells. We saw that the LepR+ barrier surrounding sympathetic AT nerves was formed of multiple, thin LepR+ cells (Figure 1E), similar to the perineurium.[14–16] To resolve their identity, we sorted LepR+ cells from the superior cervical ganglia (SCGs) of LepR^eYFP mice and performed bulk RNA sequencing (RNA-seq). Gene expression analysis revealed that these
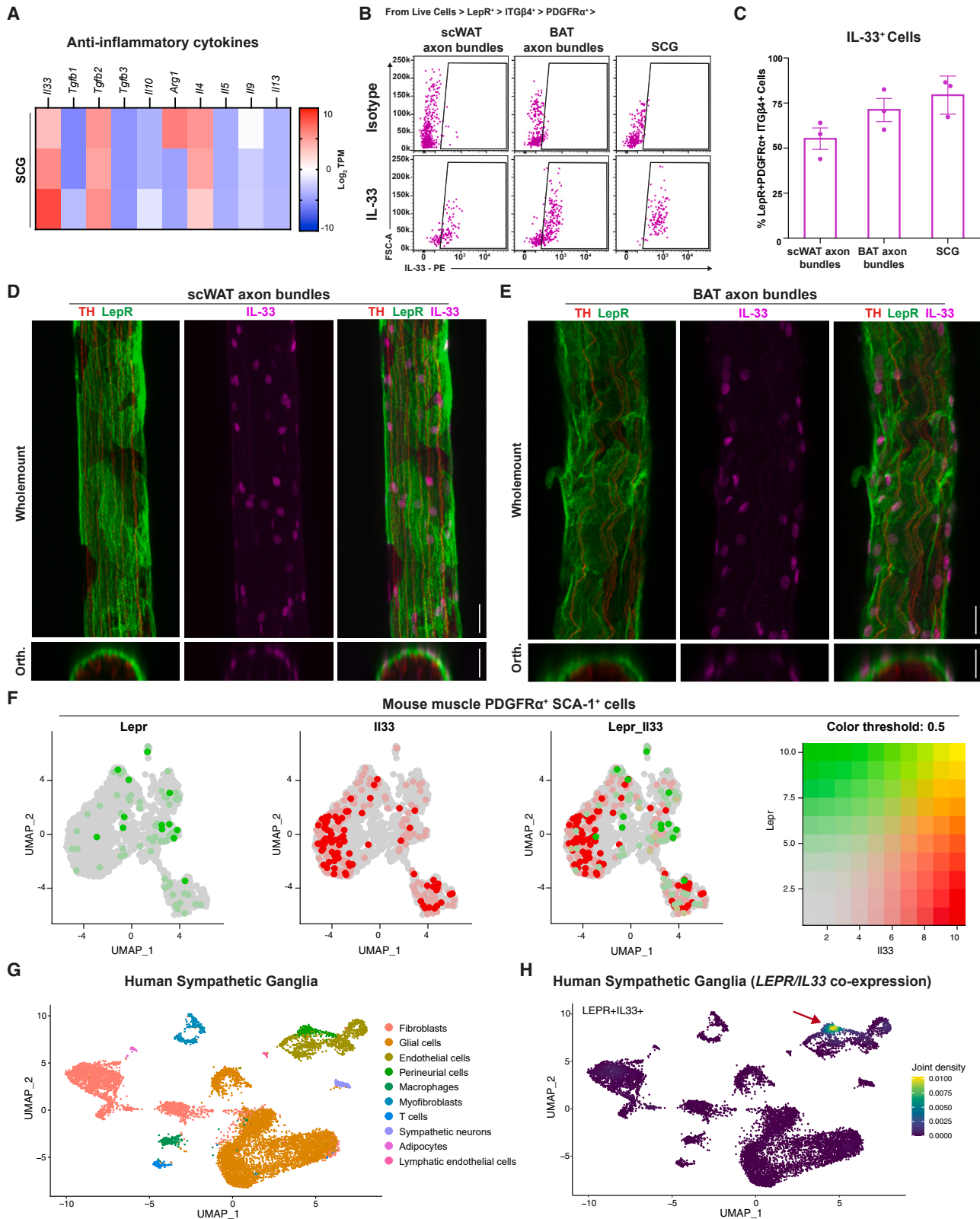
**Figure 2. LepR+ sympathetic perineural cells (SPCs) produce anti-inflammatory IL-33 in mice and humans**

(A) Bulk RNA-seq of LepR+ cells sorted from the superior cervical ganglia (SCGs) of LepR$^{eYFP}$ mice shows that LepR+ cells express anti-inflammatory cytokines, including $Il33$, $Tgfb2$, and $Il4$. n = 3, data presented as log$_2$ transcripts per million (TPM).

LepR+ cells expressed *Lepr*, a range of perineurial (*Cldn1*, *Cav1*, *Dcn*, *Igfbp6*, *Tjp1*, and *Vcl*) and mesenchymal (*Pdgfra*, *Vim*, *Pdpn*, *Cd34*, and *Ly6a*) markers, with low expression of endothelial markers (*Pecam1*, *Cdh5*, *Tek*, and *Kdr*) and an absence of expression of the epithelial markers *Epcam* and *Muc1* (Figure 1F). Using flow cytometry, we verified that the vast majority of LepR+ cells in sympathetic tissues stained positive for fibroblastic and perineurial markers, PDGFRα and ITGβ4, respectively (Figures 1G and S1B). Few LepR+ cells were positive for endothelial markers CD31 and CDH5 (Figure 1G). We, therefore, named these specialized LepR+ cells sympathetic perineurial cells (SPCs).

### LepR+ SPCs produce anti-inflammatory IL-33 in mice and humans

Having characterized LepR+ SPCs, we hypothesized they had an immunometabolic role, preventing the chronic, low-grade AT inflammation closely associated with obesity. Analysis of our RNA-seq dataset revealed high expression of anti-inflammatory cytokines interleukin-33 (*Il33*), transforming growth factor β2 (*Tgf-b2*), and interleukin-4 (*Il4*) in LepR+ SPCs (Figure 2A). Recent studies have implicated IL-33 and IL-33-responsive immune cells in the control of AT homeostasis.[19–21] Using flow cytometry, we found that the majority of LepR+ SPCs in all sympathetic tissues were IL-33+ (Figures 2B and 2C) and verified the presence of IL-33 protein in scWAT and BAT axon bundles using IF imaging (Figures 2D and 2E). Orthogonal, optical reconstructions and videos of whole-mount-imaged scWAT and BAT axon bundles revealed exclusive IL-33 staining in the outer LepR^eYFP+ perineurial barrier cells (Figures 2D and 2E; Videos S3 and S4). To determine whether *Lepr* and *Il33* co-expression is unique to SPCs in AT sympathetic axon bundles, we compared them with previously identified IL-33-producing stromal cells associated with sensory neurons in the muscle.[19,22,23] Considering that our LepR+ SPCs also expressed *Pdgfra* and *Ly6a* (Figures 1F and 1G), we analyzed the available published single-cell RNA-seq (scRNA-seq) data of PDGFRα+SCA-1+ cells sorted from mouse muscle tissue[19] and confirmed *Pdgfra* and *Ly6a* expression (Figures S2A and S2B). We found that *Lepr* and *Il33* were not co-expressed in muscle stromal cells (Figure 2F), indicating that LepR+ SPCs are a previously unreported subset of perineurial cells that ensheathes sympathetic AT axon bundles. Next, given the existence of LepR+IL-33+ SPCs in mouse sympathetic tissues, we aimed to determine whether LepR+IL-33+ SPCs exist in humans. We performed single-nuclei sequencing on sympathetic ganglia acquired from human donors, which revealed a number of stromal cell subsets and immune cell clusters alongside the expected sympathetic neurons (Figure 2G). Within human sympathetic ganglia, we observed that only the perineurial

cell cluster co-expressed *LEPR* and *IL33* (Figures 2H and S2C). Together, we show the existence of a previously unreported perineurial cell subtype associated with sympathetic tissues, which co-express *Lepr* and *Il33* in both mice and humans.

### *Lepr* and *Il33* co-expression is not observed in the hypothalamus or peripheral organs of the *Tabula Muris* database

To exclude the possibility of off-target effects for a *Lepr*^cre-mediated conditional IL-33 genetic ablation mouse model, we first assessed whether any other cell in wild-type (WT) mice is double positive for *Lepr* and *Il33*. We analyzed public scRNA-seq data from the arcuate nucleus of the hypothalamus (ARC)[24] and found that cells in the ARC did not co-express *Lepr* and *Il33* (Figure S2D), which we also confirmed using IF imaging (Figure S2E). We next assessed *Lepr* and *Il33* co-expression in peripheral organs, using the *Tabula Muris* scRNA-seq database,[25] which revealed that the kidney, muscle, and trachea were the most likely to co-express *Lepr* and *Il33*, with correlation coefficients between 0.1 and 0.4 (Figure S2F). However, IF imaging excluded the possibility of LepR+IL-33+ cells in these organs (Figure S2G). Using this method, we also excluded *Lepr* and *Il33* co-expression in the aorta, heart, and liver, with co-expression correlation coefficients of 0.08–0.1 (Figure S2F). The diaphragm, pancreas, tongue, bone marrow, skin, colon, thymus, and bladder all had very low *Lepr*/*Il33* correlation coefficients (below 0.05), and hence LepR+IL-33+ cells in these organs can be safely excluded (Figure S2F). We therefore confirm that LepR+IL-33+-expressing cells are not present in the ARC, nor in the peripheral tissues listed in the *Tabula Muris* database.

### Loss of IL33 in LepR+ SPCs drives BAT inflammation

To functionally assess the role of IL-33 on SPC cell function, we crossed *Lepr*^cre mice with *Il33*^fl/fl mice to perform a conditional genetic ablation of IL-33 only in SPCs (herein named SPC^ΔIl33 mice). Having validated that other than the SPCs, no cells in the ARC or organs of the *Tabula Muris* co-express *Lepr* and *Il33*, we next verified, using IF, that IL-33 was lost in SPCs in SPC^ΔIl33 AT axon bundles (Figures 3A and 3B) and found that lean SPC^ΔIl33 mice fed a normal diet (ND) have comparable body weights, AT weights, and food intake to *Il33*^fl/fl controls (Figures 3C–3G, S3A, and S3B). Considering the role of IL-33 in the type 2 immune response, we next tested if known IL-33-responsive (ST2+) AT immune cells—including Treg cells and eosinophils—were reliant on SPC-derived IL-33.[26–33] While the spleen and WAT depots appeared unaffected, CD45+ cell count was significantly reduced in the BAT of SPC^ΔIl33 mice (Figure 3H). Upon closer inspection, this was due to a decrease in the frequency of both Treg cells and eosinophils in the BAT (Figures 3I

(B and C) Flow cytometric analysis reveals that the majority of LepR+ SPCs (PDGFRα+ITGβ4+) in sympathetic tissues are IL-33+. LepR^eYFP mice (n = 3). Full gating strategy of LepR+ SPCs in Figure S1B. Data presented as mean ± SEM.

(D and E) LepR+ sympathetic perineurial cells (SPCs) in subcutaneous (scWAT, D) and brown (BAT, E) adipose tissue axon bundles are IL-33+. LepR^eYFP mouse, 20× maximum intensity projection images (whole mount) or orthogonal reconstruction (Orth). TH, tyrosine hydroxylase (red); LepR^eYFP (green); IL-33 (magenta). Scale bars, 25 μm.

(F) PDGFRα+SCA-1+ cells in mouse muscle, including those associated with sensory neurons,[19] do not co-express *Lepr* and *Il33*.

(G and H) Single-nuclei sequencing was performed on sympathetic ganglia from human donors. (G) Cell clusters within human stellate ganglia. (H) Joint density plot showing co-expression of *LEPR* and *IL33* within human sympathetic ganglia. *LEPR* and *IL33* are co-expressed exclusively in the perineurial cell cluster (red arrow).

See also Figure S2.
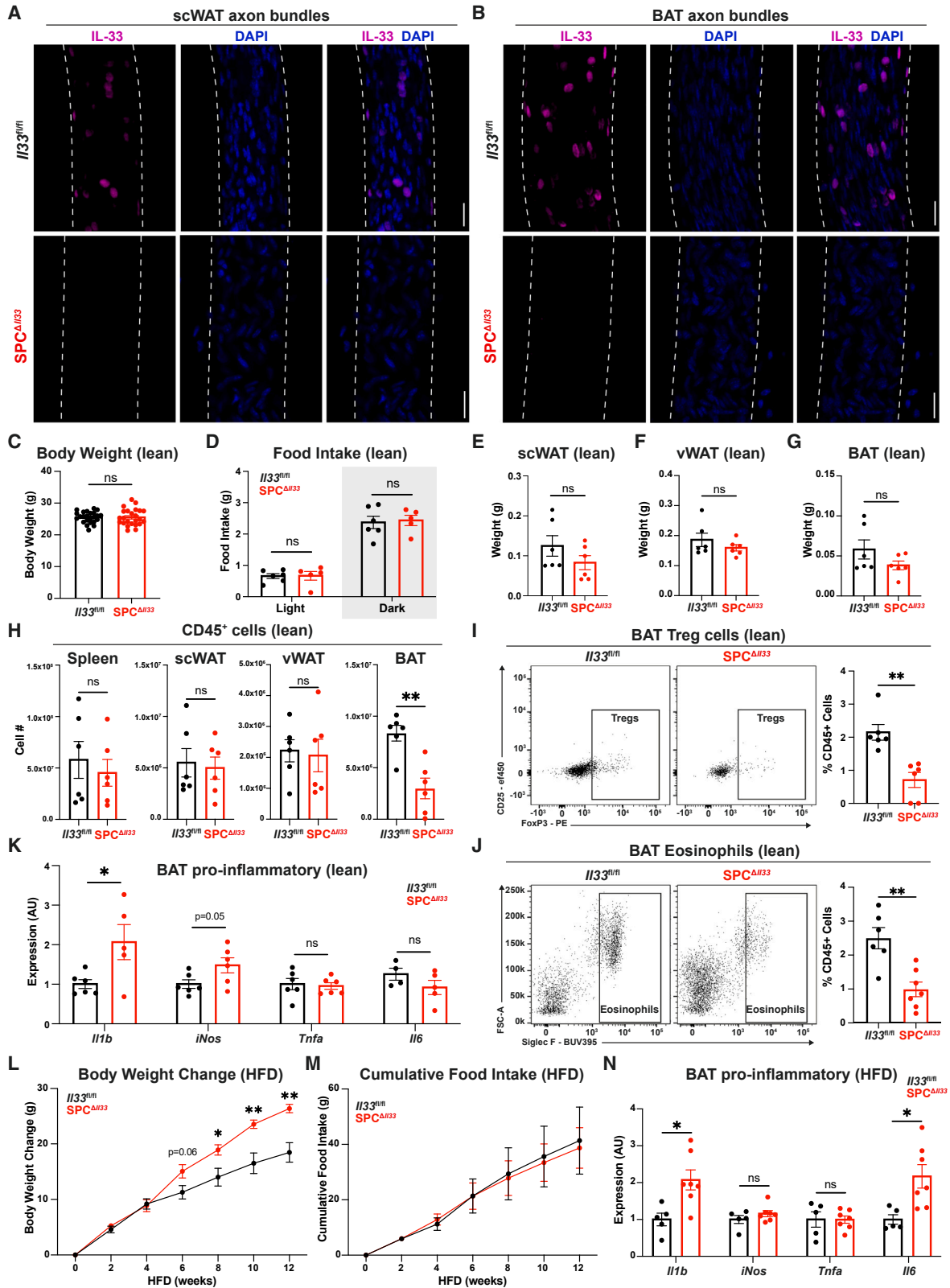
and 3J), with no significant differences in splenic or scWAT Treg cells and eosinophil frequencies (Figures S3C–S3F). While visceral white AT (vWAT) Treg cell frequency remained unchanged, a significant decrease in vWAT eosinophils was observed in SPC$^{\Delta Il33}$ mice (Figures S3D and S3F). Specifically, IL33-responsive immune cells seem to be most affected in the BAT of SPC$^{\Delta Il33}$ mice. In addition to changes in BAT-resident immune cells, we observed that the expression of *Il1b* was increased in lean SPC$^{\Delta Il33}$ BAT, indicating some inflammation (Figure 3K). In summary, we show SPC$^{\Delta Il33}$ manifests in changes to BAT immune cell recruitment and maintenance.

### Production of IL-33 by LepR+ SPCs is protective against diet-induced obesity

Although SPC$^{\Delta Il33}$ mice did not develop obesity when fed a ND, we found that SPC$^{\Delta Il33}$ mice metabolically challenged with a high-fat diet (HFD) from 8 weeks old for 12 weeks gained more weight independently of food intake, relative to age-matched, HFD-fed *Il33*$^{fl/fl}$ controls (Figures 3L, 3M, and S3G). Furthermore, HFD-fed SPC$^{\Delta Il33}$ mice had increased scWAT weights, compared with control mice, although no significant difference was observed in vWAT or BAT weights (Figures S3H–S3J). Having identified the BAT as a potential site of metabolic dysregulation in SPC$^{\Delta Il33}$ mice (Figures 3I and 3J), we also found, using qPCR, that HFD-fed SPC$^{\Delta Il33}$ BAT was more inflamed than HFD-fed control BAT, with increased expression of *Il1b* and *Il6* (Figure 3N). Collectively, this further supports a role for SPC-derived IL-33 in BAT homeostasis.

### IL-33 derived from LepR+ SPCs is required for cold-induced BAT thermogenesis

BAT is the primary site of non-shivering thermogenesis, a major process of energy expenditure. Previous work has directly implicated Treg cells and eosinophils in the induction of thermogenesis,[21,29,34] which prompted us to investigate whether the reduction in the frequency of BAT Treg cells and eosinophils in SPC$^{\Delta Il33}$ mice would impact thermogenesis. Thermal imaging and temperature measurements of lean, unchallenged SPC$^{\Delta Il33}$

and *Il33*$^{fl/fl}$ mice revealed no significant differences in BAT, core, or tail temperature (Figures 4A–4C, S4A, and S4B). Further corroborating this finding, no differences were detected in the energy expenditure and respiratory quotient of lean, unchallenged SPC$^{\Delta Il33}$ and *Il33*$^{fl/fl}$ mice (Figures 4D and S4C–S4E), and qPCR analysis of BAT confirmed no significant differences in the expression of thermogenic genes between lean, unchallenged SPC$^{\Delta Il33}$ and *Il33*$^{fl/fl}$ mice (Figure 4E). We next assessed BAT activity in cold-challenged, lean mice. We housed mice at thermoneutrality (30°C) for 10 days to reduce BAT thermogenesis, before subjecting one group to an additional 4°C cold challenge for 8 h (Figure 4F). We first confirmed the robust, cold-induced upregulation of thermogenic genes such as *Ucp1*, *Pgc1a*, *Elovl3*, *Dio2*, *Lpl*, and *Gpr3* between thermoneutral and cold-challenged WT mice (Figure 4G), before assessing differences between cold-challenged *Il33*$^{fl/fl}$ and SPC$^{\Delta Il33}$ mice (Figure 4H). Notably, SPC$^{\Delta Il33}$ mice were unable to upregulate both *Elovl3* and *Gpr3* following cold challenge (Figure 4I). *Elovl3* expression is highly correlated with recruitment of thermogenic brown adipocytes in BAT and contributes to the production of <1% of the cellular BAT lipidome.[35] Additionally, *Gpr3* encodes a constitutively active, cold-induced G2-coupled receptor in brown and inducible beige adipocytes, upregulated in response to non-canonical lipolytic signals, and has been directly correlated with energy expenditure due to its constitutive activation.[36] Together, we show that loss of IL-33 production by SPCs impairs adaptive BAT thermogenesis in metabolically challenged SPC$^{\Delta Il33}$ mice.

### IL-33 produced by SPCs is required for leptin's rescue of metabolic adaptation to fasting

Finally, we developed a protocol to induce and subsequently rescue a state of metabolic adaptation to assess the physiological role of IL-33 in SPCs. Metabolic adaptation is the reduction in energy expenditure in response to fasting to preserve energy stores, which we detected by the reduction in BAT temperature (Figures S5A and S5B). In response to a 14-h fast, we found that expression of thermogenic genes *Ucp1*, *Elovl3*, and *Dio2* was

---

**Figure 3. Loss of IL-33 in LepR+ SPCs induces brown adipose tissue inflammation and predisposes mice to obesity, independently of food intake**

(A and B) IL-33 is lost in the LepR+ sympathetic perineurial cells (SPCs) of SPC$^{\Delta Il33}$ subcutaneous (scWAT, A) and brown (BAT, B) adipose tissue axon bundles. *Il33*$^{fl/fl}$ and SPC$^{\Delta Il33}$ mice, 20× maximum intensity projection images. IL33 (magenta), DAPI (blue). Scale bars, 25 μm. White dotted lines mark nerve edges.

(C) Absolute body weight of lean (normal diet-fed) *Il33*$^{fl/fl}$ and SPC$^{\Delta Il33}$ mice. n = 24, 3 independent experiments.

(D) Average food intake per mouse of normal diet-fed *Il33*$^{fl/fl}$ and SPC$^{\Delta Il33}$ mice during light/dark periods, measured over a 5-day period. n = 5–6, 1 independent experiment.

(E–G) Comparable adipose tissue weights between lean (normal diet-fed) *Il33*$^{fl/fl}$ and SPC$^{\Delta Il33}$ mice. Subcutaneous white adipose tissue (scWAT, E), visceral white adipose tissue (vWAT, F), and brown adipose tissue (BAT, G). n = 6, 2 independent experiments.

(H) Absolute number of CD45+ cells in the spleen, subcutaneous (scWAT), visceral (vWAT), and brown adipose tissue (BAT) of *Il33*$^{fl/fl}$ and SPC$^{\Delta Il33}$ mice. n = 6, 2 independent experiments.

(I and J) Flow cytometric analysis of brown adipose tissue (BAT) from lean (normal diet-fed) *Il33*$^{fl/fl}$ and SPC$^{\Delta Il33}$ mice shows a reduction in the frequency of BAT Treg cells (I) and eosinophils (J). (I) n = 6, 2 independent experiments. (J) n = 6–7, 2 independent experiments.

(K) qPCR of BAT shows increased inflammation in lean (normal diet-fed) SPC$^{\Delta Il33}$ mice. For each gene, data are presented relative to lean *Il33*$^{fl/fl}$ expression (=1). *Il1b*, interleukin-1 beta; iNos, inducible nitric oxide synthase; *Tnfa*, tumor necrosis factor alpha; *Il6*, interleukin-6. n = 4–6, 2 independent experiments.

(L and M) SPC$^{\Delta Il33}$ mice gain more weight than *Il33*$^{fl/fl}$ controls when fed high-fat diet (HFD, L), despite no difference in food intake (M). Body weight change (L) of *Il33*$^{fl/fl}$ and SPC$^{\Delta Il33}$ mice fed HFD from 8 weeks old. n = 6, 2 independent experiments.

(N) HFD-fed SPC$^{\Delta Il33}$ mice have increased BAT inflammation, compared with HFD-fed *Il33*$^{fl/fl}$ controls. qPCR shows higher expression of pro-inflammatory genes *Il1b* and *Il6* in SPC$^{\Delta Il33}$ BAT. For each gene, data are presented relative to *Il33*$^{fl/fl}$ HFD expression (=1). *Il1b*, interleukin-1 beta; iNos, inducible nitric oxide synthase; *Tnfa*, tumor necrosis factor beta; *Il6*, interleukin-6. n = 5–7, 1 independent experiment. Data presented as mean ± SEM. Student's t test; ns, not significant; *p < 0.05 and **p < 0.01.
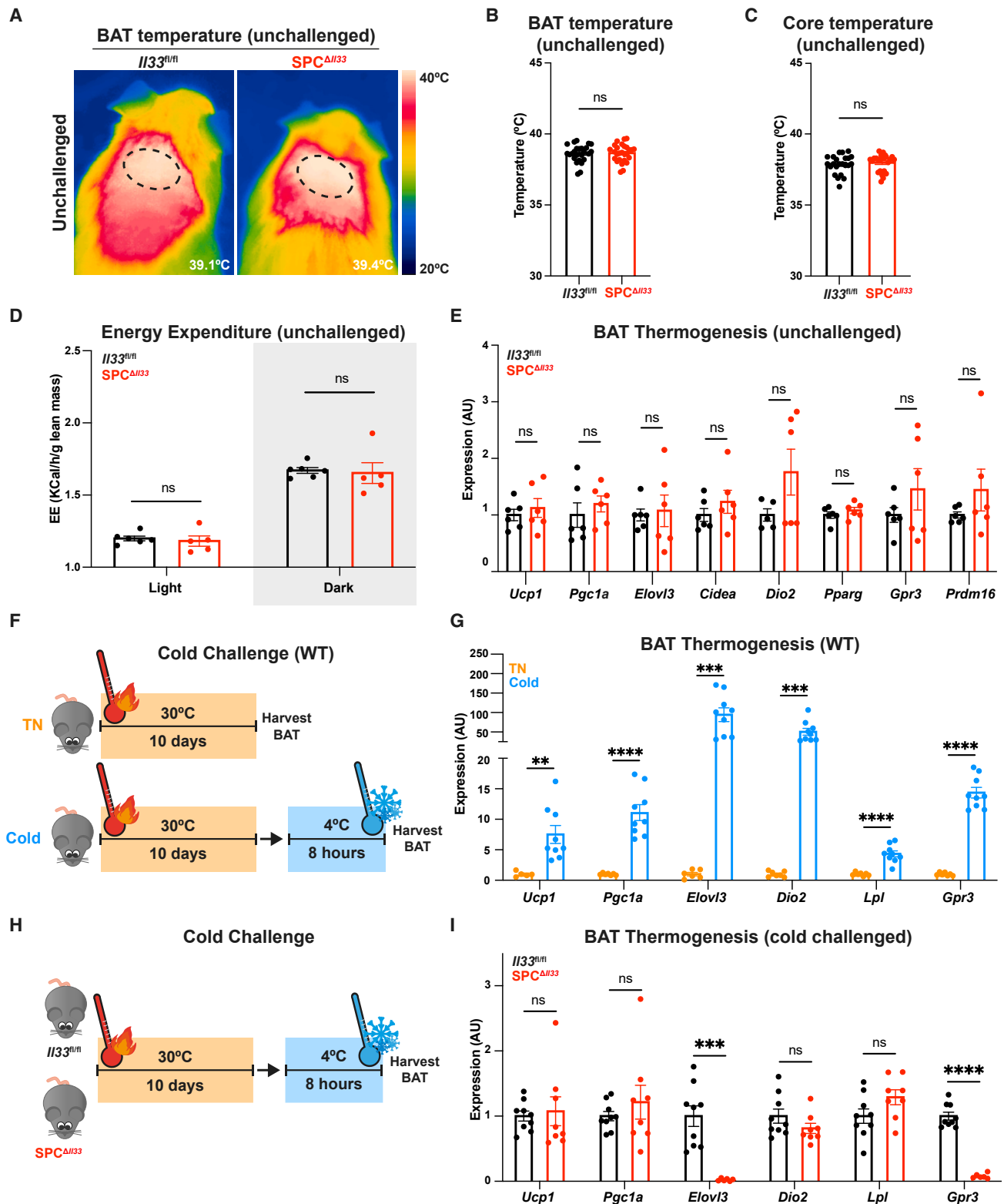
See also Figure S3.

**Figure 4. IL-33 derived from LepR+ SPCs is required for cold-induced BAT thermogenesis**

(A and B) Brown adipose tissue (BAT) temperature is comparable in lean, unchallenged SPC$^{\Delta Il33}$ and $Il33^{fl/fl}$ mice. Thermal imaging (A) and quantification (B) at room temperature (21°C). (A) Dotted lines indicate region measured; bottom right: average temperature in image shown. (B) Each data point represents average BAT temperature per mouse, calculated from <10 thermal images. n = 25–27, 4 independent experiments.

lower in SPC$^{\Delta Il33}$ BAT, compared with that in $Il33^{fl/fl}$ controls, indicating that SPC$^{\Delta Il33}$ mice exhibit a reduced capacity for thermogenesis with calorie restriction (Figure 5A). We used leptin to stimulate BAT thermogenesis and rescue the fasting-induced metabolic adaptation (Figure 5B). Indeed, we observed that relative to PBS-injected controls, leptin rescues the BAT temperature of fasted $Il33^{fl/fl}$ mice 1 h post-intraperitoneally (i.p.) injection (Figures 5C, 5D, and S5C). However, in fasted SPC$^{\Delta Il33}$ mice, we observed that the BAT temperature was not rescued by i.p. leptin injection (Figures 5E, 5F, and S5D), indicating that SPC$^{\Delta Il33}$ BAT is unresponsive to the leptin-induced stimulation of thermogenesis. Collectively, we show here that IL-33 produced by SPCs is required for BAT response to a leptin challenge and metabolic adaptation to fasting.

## DISCUSSION

Obesity research has been divided into neuroendocrinology and immunometabolism, but a link is missing between these diverse fields of study. Here, we have identified a LepR+, IL-33-producing SPC barrier surrounding sympathetic ganglia and axon bundles in ATs, providing a cellular link between these distinct fields. Across a range of different species, perineurial cells have been described as mesenchymal,[37] fibroblastic,[38,39] endothelial-like,[40] and epithelial[41]; with proposed functions including nerve protection and regeneration,[14–16,41] but they have not been previously described as LepR+. We have uncovered unforeseen hormone-sensing and immunomodulatory roles for LepR+ SPCs by showing that they are leptin-sensing and capable of signaling BAT immune cells through the production of IL-33.

The importance of IL-33-producing stromal cells for immune recruitment and maintenance has been described in a variety of tissues. In fact, Kuswanto et al.[23] and Wang et al.[22] have recently reported an IL-33+ subset of stromal cells associated with sensory neurons in muscle, which are not LepR+, based on our IF imaging analysis and analysis of available scRNA-seq. We have therefore shown that LepR+ SPCs are an anatomically and transcriptionally distinct, leptin-sensitive subset of IL-33-producing perineurial cells associated with sympathetic axon bundles in AT. Furthermore, two recent back-to-back papers

have described the heterogeneity of IL-33-producing mesenchymal cells in WAT but did not identify an IL-33-producing perineurial cell population.[19,20] We found that sympathetic axon bundles must first be dissected to isolate LepR+ SPCs, and we thus propose that these perineurial barrier cells are a source of IL-33 that is distinct from those previously reported by Māhlakoiv et al.[20] and Spallanzani et al.[19] using bulk analyses of ATs. These studies involving either a total genetic ablation of $Il33$[20] or a PDGFRα-dependent conditional genetic deletion of $Il33$ ($Pdgfra^{cre}$ x $Il33^{fl/fl}$)[19] have been crucial in understanding the role of IL-33 in AT but have focused solely on WAT and not BAT. A whole-body genetic ablation of $Il33$ results in increased weight gain in the absence of metabolic challenge, whereas a PDGFRα-driven conditional deletion of IL-33 was not sufficient to induce obesity in the unchallenged state, phenocopying SPC$^{\Delta Il33}$ mice. Furthermore, we demonstrated that the frequency of vWAT and scWAT Treg cells is unaltered in unchallenged SPC$^{\Delta Il33}$ mice, in comparison with the reduction observed in $Pdgfra^{cre}$ x $Il33^{fl/fl}$ vWAT.[19] Most notably, we show that deletion of $Il33$ in SPCs resulted in a loss of BAT-resident anti-inflammatory Treg cells and eosinophils, contributing to BAT inflammation. IL-33-mediated orchestration of immune cells by LepR+ SPCs is distinct in both mechanism and tissue from the glial-derived neurotrophic factor (GDNF)-dependent immunosignaling reported in sympathetic-associated stromal cells of the vWAT,[42] and it further reinforces a tissue-specific specialized immunomodulatory role for SPCs.

Increased adiposity with obesity results in higher circulating leptin and increased expression of pro-inflammatory cytokines by adipocytes,[43] promoting chronic, low-grade AT inflammation. Leptin itself is well described as a pro-inflammatory adipokine,[44,45] with the ability to suppress the proliferation and anti-inflammatory cytokine production of plasma-derived Treg cells ex vivo.[46] Here, we have described IL-33 production by LepR+ SPCs as a possible negative feedback "brake" on the pro-inflammatory effect of leptin in lean AT. Loss of LepR+ SPC-derived IL-33 increased BAT inflammation in both ND- and HFD-fed mice, resulting in impaired adaptive thermogenesis. We identified LepR+ SPCs as a major contributor of IL-33 to recruit and/or maintain a pool of BAT Treg

(C) Core temperature of lean SPC$^{\Delta Il33}$ mice is unaltered at room temperature (21°C). n = 22–24, 4 independent experiments.

(D) Energy expenditure (EE) is comparable in lean SPC$^{\Delta Il33}$ and $Il33^{fl/fl}$ mice. Each data point represents an average of EE per mouse during light/dark periods, measured over a 5-day period. EE normalized to lean mass. n = 5–6, 1 independent experiment.

(E) qPCR of BAT from lean $Il33^{fl/fl}$ and SPC$^{\Delta Il33}$ mice shows no difference in BAT thermogenic gene expression in unchallenged mice at room temperature (21°C). For each gene, data are presented relative to IL33$^{fl/fl}$ expression (=1). $Ucp1$, uncoupled protein 1; $Pgc1a$, peroxisome proliferator-activated receptor gamma coactivator 1-alpha; $Elovl3$, Elovl3 fatty acid elongase 3; $Cidea$, cell death-inducing DFFA-like effector A; $Dio2$, iodothyronine deiodinase 2; $Pparg$, peroxisome proliferator-activated receptor gamma; $Gpr3$, G protein-coupled receptor 3; $Prdm16$, PR/SET Domain 16. n = 6, 2 independent experiments.

(F) Schematic representation: control WT mice were housed at thermoneutrality (30°C) for a period of 10 days before tissue harvest. Cold-challenged WT mice underwent an additional 8-h cold challenge (4°C).

(G) qPCR on the brown adipose tissue of wild-type thermoneutral (TN, orange) vs. wild-type cold-challenged (cold, blue) mice shows the robust upregulation of thermogenic gene expression following cold challenge. For each gene, data are presented relative to thermoneutral expression (=1). $Ucp1$, uncoupled protein 1; $Pgc1a$, peroxisome proliferator-activated receptor gamma coactivator 1-alpha; $Elovl3$, Elovl3 fatty acid elongase 3; $Dio2$, iodothyronine deiodinase 2; $Lpl$, lipoprotein lipase; $Gpr3$, G protein-coupled receptor 3. n = 6–9, 2 independent experiments.

(H) Schematic representation: cold-challenged $Il33^{fl/fl}$ and SPC$^{\Delta Il33}$ mice were housed at thermoneutrality (30°C) for 10 days before an 8-h cold challenge (4°C).

(I) qPCR of brown adipose tissue (BAT) shows impaired $Elovl3$ and $Gpr3$ upregulation in cold-challenged SPC$^{IL33cKO}$ mice, compared with cold-challenged IL33$^{fl/fl}$ controls. For each gene, data are presented relative to cold-challenged $Il33^{fl/fl}$ expression (=1). $Ucp1$, uncoupled protein 1; $Pgc1a$, peroxisome proliferator-activated receptor gamma coactivator 1-alpha; $Elovl3$, Elovl3 fatty acid elongase 3; $Dio2$, iodothyronine deiodinase 2; $Lpl$, lipoprotein lipase; $Gpr3$, G protein-coupled receptor 3. n = 6, 2 independent experiments. Data presented as mean ± SEM. Student's t test; ns, not significant; **p < 0.01, ***p < 0.001, and ****p < 0.0001.
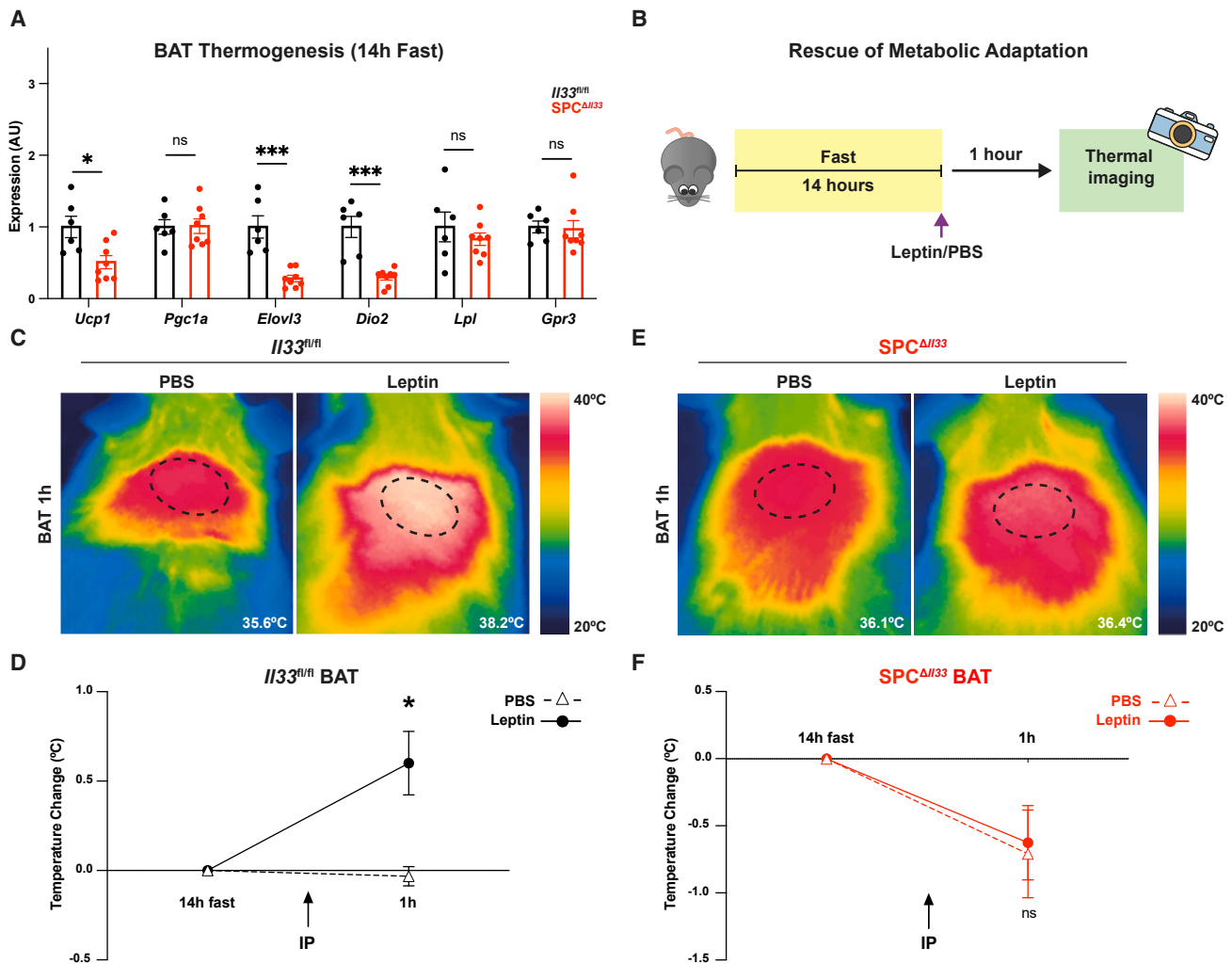
See also Figure S4.

**Figure 5. IL-33 from SPCs mediates metabolic adaptation in BAT**

(A) Expression of *Elovl3* and *Dio2* thermogenic genes are reduced in the BAT of SPC$^{\Delta Il33}$ mice fasted for 14 h, compared with 14-h fasted *Il33*$^{fl/fl}$ BAT. *Ucp1*, uncoupled protein 1; *Pgc1a*, peroxisome proliferator-activated receptor gamma coactivator 1-alpha; *Elovl3*, Elovl3 fatty acid elongase 3; *Dio2*, iodothyronine deiodinase 2; *Lpl*, lipoprotein lipase; *Gpr3*, G protein-coupled receptor 3. n = 6–8, 2 independent experiments.

(B) Leptin-induced rescue of metabolic adaptation. Mice were fasted for 14 h to induce metabolic adaptation before i.p. injection of leptin or PBS (control). BAT temperature was measured 1 h following i.p. injection.

(C–F) Leptin rescues metabolic adaptation in *Il33*$^{fl/fl}$ mice (C and D) but not in SPC$^{\Delta Il33}$ mice (E and F). Thermal images of *Il33*$^{fl/fl}$ BAT (C) and SPC$^{\Delta Il33}$ BAT (E) 1 h following i.p. injection of either leptin or PBS, representative of n = 5–6, 2 independent experiments. Dotted lines indicate region from which the average BAT temperature was measured; bottom right: average temperature in thermal image shown. (D and F) BAT temperature was measured from mice injected with either leptin (solid line) or PBS (dotted line). Presented relative to fasted BAT temperature. n = 5–6, 2 independent experiments. Data presented as mean ± SEM. (A) Student's t test; (D and F) two-way ANOVA with Šidak correction for multiple comparisons. ns, not significant; *p < 0.05 and ***p < 0.001.
See also Figure S5.

cells and eosinophils, corroborating previous reports suggesting a role in thermogenesis for these immune cells.[21,29,34] Although unchallenged SPC$^{\Delta Il33}$ mice have unaltered metabolism, dysfunction emerges upon metabolic challenge, with worsened HFD-induced obesity and impaired BAT thermogenesis in response to cold, fasting, and leptin stimulation. Collectively, we have shown that SPC-derived IL-33 is critical for BAT response to metabolic challenge, establishing a role for LepR+ SPCs in the regulation of energy homeostasis. We have uncovered SPCs as an upstream, immunomodulatory, sympathetic-associated stromal cell that is a missing link be-

tween leptin and immunometabolic mechanisms controlling body weight homeostasis and obesity.

**Limitations of the study**

ATs are highly innervated by sympathetic neurons, which have been shown to positively regulate AT lipolysis and thermogenesis through norepinephrine release in a range of loss-of-function and gain-of-function experiments.[10,47–49] Furthermore, sympathetic axon bundles innervating AT are visible under a stereomicroscope[10,17,18,47–50] and can be dissected. While every effort was made to thoroughly sample and image axon bundles within

mouse ATs to ensure fair representation, we, and others, lack the ability to confirm that individual neurons within these upstream nerve bundles directly synapse onto adipocytes, as opposed to being en passant neurons that pass through ATs to functionally innervate other peripheral organs. While the presence of LepR⁺IL-33⁺ SPCs was confirmed in females by using IF (data not shown), owing to the role of estrogen on feeding and sympathetic AT innervation,[51] only male mice were used experimentally.

## STAR★METHODS

Detailed methods are provided in the online version of this paper and include the following:

- KEY RESOURCES TABLE
- RESOURCE AVAILABILITY
  - Lead contact
  - Materials availability
  - Data and code availability
- EXPERIMENTAL MODEL AND STUDY PARTICIPANT DETAILS
  - Mice
  - Human
- METHOD DETAILS
  - Metabolic phenotyping
  - High fat diet challenge
  - Cold challenge
  - Fasting and rescue of metabolic adaptation
  - Temperature measurements
  - Immunofluorescence and confocal microscopy
  - Transmission electron microscopy
  - Mouse Single cell suspensions
  - Flow cytometry
  - Mouse SCG LepR⁺ cell bulk RNA seq
  - Human ganglia single nuclei RNA-seq
  - Published single-cell RNA sequencing analysis
  - RNA extraction, cDNA generation and qPCR
- QUANTIFICATION AND STATISTICAL ANALYSIS

### SUPPLEMENTAL INFORMATION

Supplemental information can be found online at https://doi.org/10.1016/j.immuni.2023.11.006.

### AUTHOR CONTRIBUTIONS

A.I.D. conceptualized the study. B.A.A. first visualized LepR⁺ SPCs, B.A.A., S.Y.-Ö., and N.M.-S. sorted LepR⁺ cells from SCG, which were sequenced by S.C. and F.G. at SIgN Immunogenomic core, A*STAR. Transmission electron microscopy was performed by A.R. and M.I. on samples prepared by B.A.A. and N.M.-S. S.Y.-Ö. created the first generations of SPC^{Δil33} mice. Flow cytometry was performed by E.R.H. with the help of S.Y.-Ö., C.J.O.O., and C.Z. Sample preparation and confocal microscopy was performed by E.R.H., G.S., and E.F. Analyses of published scRNA-seq data was performed by E.R.H., G.S., D.E.G., and D.S.-O. Metabolic phenotyping and subsequent analyses were performed by I.F.-G. and M.L. Weight acquisition (normal diet and high-fat diet) and fasting were perfomed by E.R.H. Cold challenge, leptin-induced rescue of metabolic adaptation, and accompanying thermal imaging were performed by E.R.H with the help of G.S. qPCR experiments were performed by E.R.H. G.S. purchased and helped set up the cold chambers to meet H.O. standards. Blinded thermal imaging analyses were performed by E.R.H. and E.F. Single-nuclei sequencing and subsequent analysis of human sympathetic ganglia was performed by K.A.Z., S.M., and S.E. E.R.H. created the graphical abstract and wrote the first draft of the manuscript, and A.I.D. wrote the final version after several rounds of rewriting with E.R.H.

### DECLARATION OF INTERESTS

The authors declare no competing interests.

### REFERENCES

1. O'Brien, C.J.O., Haberman, E.R., and Domingos, A.I. (2021). A tale of three systems: toward a neuroimmunoendocrine model of obesity. Annu. Rev. Cell Dev. Biol. 37, 549–573.

2. Weisberg, S.P., McCann, D., Desai, M., Rosenbaum, M., Leibel, R.L., and Ferrante, A.W. (2003). Obesity is associated with macrophage accumulation in adipose tissue. J. Clin. Invest. 112, 1796–1808.

3. Pirzgalska, R.M., Seixas, E., Seidman, J.S., Link, V.M., Sánchez, N.M., Mahú, I., Mendes, R., Gres, V., Kubasova, N., Morris, I., et al. (2017). Sympathetic neuron-associated macrophages contribute to obesity by importing and metabolizing norepinephrine. Nat. Med. 23, 1309–1318.

4. Xu, H., Barnes, G.T., Yang, Q., Tan, G., Yang, D., Chou, C.J., Sole, J., Nichols, A., Ross, J.S., Tartaglia, L.A., et al. (2003). Chronic inflammation in fat plays a crucial role in the development of obesity-related insulin resistance. J. Clin. Invest. 112, 1821–1830.

5. Feuerer, M., Herrero, L., Cipolletta, D., Naaz, A., Wong, J., Nayer, A., Lee, J., Goldfine, A.B., Benoist, C., Shoelson, S., et al. (2009). Lean, but not obese, fat is enriched for a unique population of regulatory T cells that affect metabolic parameters. Nat. Med. 15, 930–939.

6. Wu, D., Molofsky, A.B., Liang, H.E., Ricardo-Gonzalez, R.R., Jouihan, H.A., Bando, J.K., Chawla, A., and Locksley, R.M. (2011). Eosinophils sustain adipose alternatively activated macrophages associated with glucose homeostasis. Science 332, 243–247.

7. Camell, C.D., Sander, J., Spadaro, O., Lee, A., Nguyen, K.Y., Wing, A., Goldberg, E.L., Youm, Y.H., Brown, C.W., Elsworth, J., et al. (2017). Inflammasome-driven catecholamine catabolism in macrophages blunts lipolysis during ageing. Nature 550, 119–123.

8. Wolf, Y., Boura-Halfon, S., Cortese, N., Haimon, Z., Sar Shalom, H.S., Kuperman, Y., Kalchenko, V., Brandis, A., David, E., Segal-Hayoun, Y.,

et al. (2017). Brown-adipose-tissue macrophages control tissue innervation and homeostatic energy expenditure. Nat. Immunol. *18*, 665–674.

9. Zhang, Y., Proenca, R., Maffei, M., Barone, M., Leopold, L., and Friedman, J.M. (1994). Positional cloning of the mouse obese gene and its human homologue. Nature *372*, 425–432.

10. Zeng, W., Pirzgalska, R.M., Pereira, M.M.A., Kubasova, N., Barateiro, A., Seixas, E., Lu, Y.H., Kozlova, A., Voss, H., Martins, G.G., et al. (2015). Sympathetic neuro-adipose connections mediate leptin-driven lipolysis. Cell *163*, 84–94.

11. Friedman, J.M., and Halaas, J.L. (1998). Leptin and the regulation of body weight in mammals. Nature *395*, 763–770.

12. Martinez-Sanchez, N., Sweeney, O., Sidarta-Oliveira, D., Caron, A., Stanley, S.A., and Domingos, A.I. (2022). The sympathetic nervous system in the 21st century: neuroimmune interactions in metabolic homeostasis and obesity. Neuron *110*, 3597–3626.

13. Domingos, A.I. (2020). Leptin: a missing piece in the immunometabolism puzzle. Nat. Rev. Immunol. *20*, 3.

14. Krnjević, K. (1954). The connective tissue of the frog sciatic nerve. Q. J. Exp. Physiol. Cogn. Med. Sci. *39*, 55–72.

15. Zochodne, D.W. (2008). Neurobiology of Peripheral Nerve Regeneration (Cambridge University Press).

16. Piña-Oviedo, S., and Ortiz-Hidalgo, C. (2008). The normal and neoplastic perineurium: a review. Adv. Anat. Pathol. *15*, 147–164.

17. Cao, Y., Wang, H., and Zeng, W. (2018). Whole-tissue 3D imaging reveals intra-adipose sympathetic plasticity regulated by NGF-TrkA signal in cold-induced beiging. Protein Cell *9*, 527–539.

18. Chi, J., Wu, Z., Choi, C.H.J., Nguyen, L., Tegegne, S., Ackerman, S.E., Crane, A., Marchildon, F., Tessier-Lavigne, M., and Cohen, P. (2018). Three-dimensional adipose tissue imaging reveals regional variation in beige fat biogenesis and PRDM16-dependent sympathetic neurite density. Cell Metab. *27*, 226–236.e3.

19. Spallanzani, R.G., Zemmour, D., Xiao, T., Jayewickreme, T., Li, C., Bryce, P.J., Benoist, C., and Mathis, D. (2019). Distinct immunocyte-promoting and adipocyte-generating stromal components coordinate adipose tissue immune and metabolic tenors. Sci. Immunol. *4*, 3658.

20. Mahlakõiv, T., Flamar, A.L., Johnston, L.K., Moriyama, S., Putzel, G.G., Bryce, P.J., and Artis, D. (2019). Stromal cells maintain immune cell homeostasis in adipose tissue via production of interleukin-33. Sci. Immunol. *4*, eaax0416.

21. Goldberg, E.L., Shchukina, I., Youm, Y.H., Ryu, S., Tsusaka, T., Young, K.C., Camell, C.D., Dlugos, T., Artyomov, M.N., and Dixit, V.D. (2021). IL-33 causes thermogenic failure in aging by expanding dysfunctional adipose ILC2. Cell Metab. *33*, 2277–2287.e5.

22. Wang, K., Yaghi, O.K., Spallanzani, R.G., Chen, X., Zemmour, D., Lai, N., Chiu, I.M., Benoist, C., and Mathis, D. (2020). Neuronal, stromal, and T-regulatory cell crosstalk in murine skeletal muscle. Proc. Natl. Acad. Sci. USA *117*, 5402–5408.

23. Kuswanto, W., Burzyn, D., Panduro, M., Wang, K.K., Jang, Y.C., Wagers, A.J., Benoist, C., and Mathis, D. (2016). Poor repair of skeletal muscle in aging mice reflects a defect in local, interleukin-33-dependent accumulation of regulatory T cells. Immunity *44*, 355–367.

24. Campbell, J.N., Macosko, E.Z., Fenselau, H., Lyubetskaya, A., Tenen, D., Goldman, M., Verstegen, A.M.J., Resch, J.M., Mccarroll, S.A., Rosen, E.D., et al. (2017). A molecular census of arcuate hypothalamus and median eminence cell types. Nat. Neurosci. *20*, 484–496.

25. Tabula Muris Consortium; Overall coordination; Logistical coordination; Organ collection and processing; Library preparation and sequencing; Computational data analysis; Cell type annotation; Writing group; Supplemental text writing group; Principal investigators (2018). Single-cell transcriptomics of 20 mouse organs creates a Tabula Muris. Nature *562*, 367–372.

26. Miller, A.M., Asquith, D.L., Hueber, A.J., Anderson, L.A., Holmes, W.M., McKenzie, A.N., Xu, D., Sattar, N., McInnes, I.B., and Liew, F.Y. (2010). Interleukin-33 induces protective effects in adipose tissue inflammation during obesity in mice. Circ. Res. *107*, 650–658.

27. Molofsky, A.B., Nussbaum, J.C., Liang, H.E., Van Dyken, S.J.V., Cheng, L.E., Mohapatra, A., Chawla, A., and Locksley, R.M. (2013). Innate lymphoid type 2 cells sustain visceral adipose tissue eosinophils and alternatively activated macrophages. J. Exp. Med. *210*, 535–549.

28. Molofsky, A.B., Van Gool, F., Liang, H.E., Van Dyken, S.J., Nussbaum, J.C., Lee, J., Bluestone, J.A., and Locksley, R.M. (2015). Interleukin-33 and interferon-Γ counter-regulate group 2 innate lymphoid cell activation during immune perturbation. Immunity *43*, 161–174.

29. Brestoff, J.R., Kim, B.S., Saenz, S.A., Stine, R.R., Monticelli, L.A., Sonnenberg, G.F., Thome, J.J., Farber, D.L., Lutfy, K., Seale, P., et al. (2015). Group 2 innate lymphoid cells promote beiging of white adipose tissue and limit obesity. Nature *519*, 242–246.

30. Brestoff, J.R., and Artis, D. (2015). Immune regulation of metabolic homeostasis in health and disease. Cell *161*, 146–160.

31. Vasanthakumar, A., Moro, K., Xin, A., Liao, Y., Gloury, R., Kawamoto, S., Fagarasan, S., Mielke, L.A., Afshar-Sterle, S., Masters, S.L., et al. (2015). The transcriptional regulators IRF4, BATF and IL-33 orchestrate development and maintenance of adipose tissue-resident regulatory T cells. Nat. Immunol. *16*, 276–285.

32. Halim, T.Y.F., Rana, B.M.J., Walker, J.A., Kerscher, B., Knolle, M.D., Jolin, H.E., Serrao, E.M., Haim-Vilmovsky, L., Teichmann, S.A., Rodewald, H.R., et al. (2018). Tissue-restricted adaptive type 2 immunity is orchestrated by expression of the costimulatory molecule OX40L on group 2 innate lymphoid cells. Immunity *48*, 1195–1207.e6.

33. Li, C., DiSpirito, J.R., Zemmour, D., Spallanzani, R.G., Kuswanto, W., Benoist, C., and Mathis, D. (2018). TCR transgenic mice reveal stepwise, multi-site acquisition of the distinctive fat-Treg phenotype. Cell *174*, 285–299.e12.

34. Medrikova, D., Sijmonsma, T.P., Sowodniok, K., Richards, D.M., Delacher, M., Sticht, C., Gretz, N., Schafmeier, T., Feuerer, M., and Herzig, S. (2015). Brown adipose tissue harbors a distinct sub-population of regulatory T cells. PLoS One *10*, e0118534.

35. Westerberg, R., Månsson, J.E., Golozoubova, V., Shabalina, I.G., Backlund, E.C., Tvrdik, P., Retterstøl, K., Capecchi, M.R., and Jacobsson, A. (2006). ELOVL3 is an important component for early onset of lipid recruitment in brown adipose tissue. J. Biol. Chem. *281*, 4958–4968.

36. Sveidahl Johansen, O., Ma, T., Hansen, J.B., Markussen, L.K., Schreiber, R., Reverte-Salisa, L., Dong, H., Christensen, D.P., Sun, W., Gnad, T., et al. (2021). Lipolysis drives expression of the constitutively active receptor GPR3 to induce adipose thermogenesis. Cell *184*, 3502–3518.e33.

37. Carr, M.J., Toma, J.S., Johnston, A.P.W., Steadman, P.E., Yuzwa, S.A., Mahmud, N., Frankland, P.W., Kaplan, D.R., and Miller, F.D. (2019). Mesenchymal precursor cells in adult nerves contribute to mammalian tissue repair and regeneration. Cell Stem Cell *24*, 240–256.e9.

38. Thomas, P.K., and Bhagat, S. (1978). The effect of extraction of the intrafascicular contents of peripheral nerve trunks on perineurial structure. Acta Neuropathol. *43*, 135–141.

39. Berthold, C.H., Fraher, J.P., King, R.H.M., and Rydmark, M. (2005). Microscopic anatomy of the peripheral nervous system. In Peripheral Neuropathy, *1* (Elsevier), pp. 35–91.

40. Key, A., and Retzius, G. (1876). Studien in der Anatomie des Nervensystems und des Bindegewebes2 (Samson & Wallin). https://collections.nlm.nih.gov/catalog/nlm:nlmuid-66211410RX2-mvpart.

41. Shanthaveerappa, T.R., and Bourne, G.H. (1964). The perineural epithelium of sympathetic nerves and ganglia and its relation to the pia arachnoid of the central nervous system and perineural epithelium of the peripheral nervous system. Z. Zellforsch. Mikrosk. Anat. *61*, 742–753.

42. Cardoso, F., Klein Wolterink, R.G.J., Godinho-Silva, C., Domingues, R.G., Ribeiro, H., da Silva, J.A., Mahú, I., Domingos, A.I., and Veiga-Fernandes, H. (2021). Neuro-mesenchymal units control ILC2 and obesity via a brain-adipose circuit. Nature *597*, 410–414.

43. Sartipy, P., and Loskutoff, D.J. (2003). Monocyte chemoattractant protein 1 in obesity and insulin resistance. Proc. Natl. Acad. Sci. USA *100*, 7265–7270.

44. Shen, J., Sakaida, I., Uchida, K., Terai, S., and Okita, K. (2005). Leptin enhances TNF-alpha production via p38 and JNK MAPK in LPS-stimulated Kupffer cells. Life Sci. *77*, 1502–1515.

45. Faggioni, R., Jones-Carson, J., Reed, D.A., Dinarello, C.A., Feingold, K.R., Grunfeld, C., and Fantuzzi, G. (2000). Leptin-deficient (ob/ob) mice are protected from T cell-mediated hepatotoxicity: role of tumor necrosis factor $\alpha$ and IL-18. Proc. Natl. Acad. Sci. USA *97*, 2367–2372.

46. De Rosa, V., Procaccini, C., Calı', G., Pirozzi, G., Fontana, S., Zappacosta, S., La Cava, A., and Matarese, G. (2007). A key role of leptin in the control of regulatory T cell proliferation. Immunity *26*, 241–255.

47. Chi, J., Crane, A., Wu, Z., and Cohen, P. (2018). Adipo-clear: a tissue clearing method for three-dimensional imaging of adipose tissue. J. Vis. Exp. 1–9.

48. Huesing, C., Qualls-Creekmore, E., Lee, N., François, M., Torres, H., Zhang, R., Burk, D.H., Yu, S., Morrison, C.D., Berthoud, H., et al. (2020). Sympathetic innervation of inguinal white adipose tissue in the mouse. J. Comp. Neurol. *529*, 1465–1485.

49. François, M., Torres, H., Huesing, C., Zhang, R., Saurage, C., Lee, N., Qualls-Creekmore, E., Yu, S., Morrison, C.D., Burk, D., et al. (2019). Sympathetic innervation of the interscapular brown adipose tissue in mouse. Ann. N. Y. Acad. Sci. *1454*, 3–13.

50. Wang, P., Loh, K.H., Wu, M., Morgan, D.A., Schneeberger, M., Yu, X., Chi, J., Kosse, C., Kim, D., Rahmouni, K., et al. (2020). A leptin–BDNF pathway regulating sympathetic innervation of adipose tissue. Nature *583*, 839–844.

51. López, M., and Tena-Sempere, M. (2015). Estrogens and the control of energy homeostasis: a brain perspective. Trends Endocrinol. Metab. *26*, 411–421.

52. Milbank, E., Dragano, N.R.V., González-García, I., Garcia, M.R., Rivas-Limeres, V., Perdomo, L., Hilairet, G., Ruiz-Pino, F., Mallegol, P., Morgan, D.A., et al. (2021). Small extracellular vesicle-mediated targeting of hypothalamic AMPK$\alpha$1 corrects obesity through BAT activation. Nat. Metab. *3*, 1415–1431.

53. Picelli, S., Faridani, O.R., Björklund, A.K., Winberg, G., Sagasser, S., and Sandberg, R. (2013). Full-length RNA-seq from single cells using Smart-seq2. Nat. Protoc. *9*, 171–181.

54. Hao, Y., Hao, S., Andersen-Nissen, E., Mauck, W.M., Zheng, S., Butler, A., Lee, M.J., Wilk, A.J., Darby, C., Zager, M., et al. (2021). Integrated analysis of multimodal single-cell data. Cell *184*, 3573–3587.e29.

**CellPress**

# STAR★METHODS

## KEY RESOURCES TABLE

| REAGENT or RESOURCE | SOURCE | IDENTIFIER |
| --- | --- | --- |
| **Antibodies** | | |
| Chicken-anti-GFP | Abcam | Cat# Ab13970 |
| Rabbit-anti-TH | Sigma | Cat# Ab152 |
| Rabbit-anti-B3-TUBULIN | Abcam | Cat# Ab18207 |
| Goat-anti-IL-33 | R&D Systems | Cat# AF3626 |
| Donkey-anti-Chicken-AF488 | Jackson Immunoresearch | Cat# 703-545-155 |
| Donkey-anti-Rabbit-AF546 | Thermofisher | Cat# A10040 |
| Donkey-anti-Goat-AF647 | Life Tech | Cat# A-21447 |
| Rabbit-anti-GFP | Invitrogen | Cat# A-11122 |
| Anti-rabbit-nanogold particles | Nanoprobes | Cat# 2003 |
| Fc block | BD Biosciences | Cat# 553142 |
| Anti-CD45-AF700 | Biolegend | Cat# 103128 |
| Anti-CD31-Pacific blue | Biolegend | Cat# 102421 |
| Anti-TER119-BUV496 | BD Biosciences | Cat# 741079 |
| Anti-PDGFRα-APC | Biolegend | Cat# 135907 |
| Anti-ITGβ4-AF405 | Thermofisher | Cat# FAB405V |
| Anti-CDH5-PE-Cy7 | Biolegend | Cat# 138015 |
| Anti-CD3e-PE-Cy5 | Biolegend | Cat# 100309 |
| Anti-CD4-BV650 | Biolegend | Cat# 100545 |
| Anti-CD8a-BV785 | Biolegend | Cat# 100749 |
| Anti-CD25-ef450 | eBioscience | Cat# 48-0251-80 |
| Anti-CD11b-ef450 | Thermofisher | Cat# 48-0112-82 |
| Anti-CD64-PE | Biolegend | Cat# 139303 |
| Anti-Siglec F-BUV395 | BD Biosciences | Cat# 740280 |
| Anti-IL-33-PE | R&D Systems | Cat# IC3626P |
| Anti-FOXP3-PE | Thermofisher | Cat# 12-5773-82 |
| Rat IgG2a kappa isotype control-PE | Thermofisher | Cat# 12-4321-83 |
| **Chemicals, peptides, and recombinant proteins** | | |
| Recombinant leptin | Bio-Techne (R&D Systems) | Cat# 498-OB-05M |
| Anti-fade media | Invitrogen | Cat# P36930 |
| Sytox blue | Thermofisher | Cat# S34857 |
| Collagenase II | Sigma | Cat# C6885 |
| Hyaluronidase IV-S | Sigma | Cat# H3884 |
| Collagenase I | Sigma | Cat# C2674 |
| Trypsin 0.25% | Thermofisher | Cat# 25200072 |
| DNAse | New England Biolabs | Cat# B0303s/M0303s |
| SuperScript II Reverse Transcriptase | Invitrogen | Cat# 18064-014 |
| **Critical commercial assays** | | |
| Aqua Live/Dead stain | Invitrogen | Cat# L34957 |
| Near IR Live/Dead stain | Invitrogen | Cat# L34975 |
| FOXP3 Fix/ Permeabilisation Kit | eBioscience | Cat# 00-5523-00 |
| Power SYBR Green Master Mix | Thermofisher | Cat# 4367659 |
| **Deposited data** | | |
| Bulk RNA sequencing data of mouse SCG | This paper | GEO, GSE227493 |
| Single cell RNA sequencing of mouse hypothalamus | Campbell et al.[24] | GEO, GSE93374 |

**Continued**

| REAGENT or RESOURCE | SOURCE | IDENTIFIER |
|---|---|---|
| *Tabula Muris* Single Cell RNA Sequencing database | Tabula Muris Consortium et al.[25] | GEO, GSE127005 |
| Single cell RNA sequencing of mouse muscle stromal cells | Spallanzani et al.[19] | GEO, GSE127005 |
| Experimental models: Organisms/strains | | |
| *Lepr^cre* mouse: B6.129(Cg)-Lepr^tm2(cre)Rck/J | The Jackson Laboratories | Strain #008320 |
| *Rosa26*^LSL-Chr2-eYFP (Ai32) mouse: B6;129S-Gt(ROSA)26Sort^m32(CAG-COP4∗H134R/EYFP)Hze/J | The Jackson Laboratories | Strain #012569 |
| *Il33*^fl/fl mouse: B6(129S4)-Il33^tm1.1Bryc/J | The Jackson Laboratories | Strain #030619 |
| Oligonucleotides | | |
| See Table S1 (Primer Sequences) | | N/A |
| Software and algorithms | | |
| Seurat | https://satijalab.org/seurat/ | Version 5 |
| Cell Ranger | 10x genomics | Version 6.0.1 |
| Nebulosa (R package) | https://github.com/powellgenomicslab/Nebulosa | Version 0.99.92 |
| FlowJo | https://www.flowjo.com | Version 10.7.1 |
| Fiji | https://fiji.sc | Version 2.14.0 |
| Flir Tools | https://www.flir.co.uk/support/products/flir-tools-plus/#Overview | N/A |
| Graphpad Prism | https://www.graphpad.com/ | Version 9 |
| Other | | |
| High fat diet (60% fat) | Research Diets | Cat#D12492 |

## RESOURCE AVAILABILITY

### Lead contact
Further information and requests for resources and reagents should be directed to and will be fulfilled by the lead contact, Prof Ana Domingos (ana.domingos@dpag.ox.ac.uk).

### Materials availability
Materials are available upon request from the lead author. This study did not generate new unique reagents.

### Data and code availability
Single-nuclei RNA-seq and bulk RNA-seq data have been deposited at GEO and are publicly available as of the date of publication. This paper analyses existing, publicly available single cell RNA sequencing data. Accession numbers for all datasets are listed in the key resources table. Other data reported in this paper is available from the lead contact upon request.

This paper does not report original code.

Any additional information required to reanalyse the data reported in this paper is available from the lead contact upon request.

## EXPERIMENTAL MODEL AND STUDY PARTICIPANT DETAILS

Mice were used as an experimental research model. Human sympathetic ganglia were used for single nuclei RNA-sequencing. Publicly available mouse single cell RNA-seq datasets were also analysed. Further details are provided in the method details section.

### Mice
LepR^eYFP lineage-tracer and SPC^ΔIl33 mice were generated by crossing *Lepr^cre* mice (Jax #008320) with either *Rosa26*^LSL-Chr2-eYFP (Jax #012569) or *Il33*^fl/fl (Jax #030619) mice, respectively. All strains used are on the C57BL/6 background. Animals were bred and maintained at the University of Oxford under specific pathogen free conditions, on a 12h light/dark cycle at 21°C+/-1°C, 50% humidity +/-10%. Owing to the effect of oestrogen on feeding and sympathetic adipose tissue innervation[51] only age-matched male mice were used, and were randomly assigned to experimental groups based on genotype (where applicable). Lean mice were 10-11 weeks old, and unless otherwise stated (e.g., 14h fast) had *ad libitum* access to regular chow diet (normal diet, ND). All experiments were performed according to University of Oxford Institutional and UK Home Office regulations and the University of Santiago de Compostela Ethical Committee (15012/2020/010).

### Human

Nuclei were isolated from frozen human sympathetic ganglion tissue collected during autopsy. Details of 2 human donors are as follows:

35 year old male, BMI = 33.77.

50 year old female, BMI = 22.95.

Approval of the responsible ethics committee (reference ID: 262/19 S-SR, Ethikkommission der Fakultät für Medizin, Technical University of Munich) was obtained.

## METHOD DETAILS

### Metabolic phenotyping

To assess the role of SPC-derived IL-33 in adipose tissue, the metabolism of 10wo ND-fed $Il33^{fl/fl}$ and SPC$^{\Delta Il33}$ was measured using indirect calorimetry (LabMaster, TSE Systems, Bad Homburg, Germany) as previously described.[52] This system is an open circuit instrument which determines $O_2$ consumption (VO$_2$), $CO_2$ production (VCO$_2$), Respiratory Quotient (RQ) - using the equation RQ=RER=VCO$_2$/VO$_2$ - and Energy Expenditure (EE). Mice were placed for 1 week prior to measurement for adaptation and measured over a period of 5 days. Nuclear Magnetic Resonance imaging (Whole Body Composition Analyser, EchoMRI) was used to measure body composition. Respiratory quotient and energy expenditure were normalised to lean mass.

### High fat diet challenge

To metabolically challenge mice, from 8 weeks old they were given *ad libitum* access to a high fat diet (60% fat, D12492: Research Diets) for a period of 12 weeks. Mouse body weight and food intake was measured throughout.

### Cold challenge

To reduce sympathetic activity onto BAT, 10wo $Il33^{fl/fl}$ and SPC$^{\Delta Il33}$ mice were housed at thermoneutrality (30°C, HPP1060 Memmert climate chamber) for 10 days with *ad libitum* access to food and water. Thermoneutral control samples were collected, before experimental mice were housed at 4°C (HPP1060 Memmert climate chamber) for 8h and cold-challenged samples were collected. Thermoneutral and cold-challenged samples were collected at the same time of day, and immediately snap frozen. All mice were culled using $CO_2$ (unperfused).

### Fasting and rescue of metabolic adaptation

To induce metabolic adaptation 10wo $Il33^{fl/fl}$ and SPC$^{\Delta Il33}$ mice were fasted for 14h, with *ad libitum* access to water. Mice were then injected intraperitoneally (IP) with either 1x PBS or 0.5mg/ml Leptin (10ul/g, BioTechne, Cat# 498-OB-05M).

### Temperature measurements

BAT and tail temperature of unanaesthetised 10wo $Il33^{fl/fl}$ and SPC$^{\Delta Il33}$ mice were measured using a thermal camera (Flir). Mice were shaved to expose the interscapular region >2 days prior to thermal imaging to avoid stress-induced BAT activity. Average temperature was calculated using Flir Tools software, where the average temperature was measured from a minimum of 10 images per mouse/ timepoint. All thermal image analysis was blinded. Core temperature was measured using a small rectal probe (Precision) on unanaesthetised mice.

### Immunofluorescence and confocal microscopy

10wo LepR$^{eYFP}$ $Il33^{fl/fl}$ and SPC$^{\Delta Il33}$ mice were given an IP overdose of pentobarbitone and perfused with 1x PBS, before dissection and fixation in 4% PFA (Thermofisher) overnight (4°C). Adipose tissue axon bundles were stained and imaged wholemount. For sectioned tissues, samples were incubated in 30% sucrose (Sigma) overnight (for brains 5 days), before being embedded in OCT, snap frozen and cryosectioned (15μm) using a Bright OTF5000 Cryostat. Wholemount and sectioned tissues were incubated in a blocking/permeabilisation buffer (3% BSA, 2% donkey serum, 1% Triton X-100, 0.1% Sodium Azide in 1x PBS) for 1h at room temperature. Overnight incubation with primary antibodies diluted in blocking/permeabilisation buffer (GFP – 1:1000 Ab13970 Abcam, TH – 1:1000 Ab152 Sigma, B3-TUB – 1:1000 Ab18207 Abcam, IL-33 – 1:50 AF3626 R&D Systems) were performed overnight at 4°C. Following washes with PBS, samples were incubated with secondary antibodies diluted 1:500 and DAPI (1:1000) in blocking/permeabilisation buffer (Dk-a-Ch-AF488 – 703-545-155 Jackson Immunoresearch, Dk-a-Rb-AF546 – A10040 Thermofisher, Dk-a-Gt-AF647 – A-21447 Life Tech) for 1h at room temperature. Samples were washed with PBS before being mounted with anti-fade medium (P36930, Invitrogen). Secondary only, DAPI-stained controls were used to ensure staining specificity. Z stack images were acquired using the LSM-880 confocal microscope. Images were visualised using Fiji.

### Transmission electron microscopy

10wo LepR$^{eYFP}$ mice were given an IP overdose of pentobarbitone and perfused with 1x PBS. Axon bundles were dissected from the subcutaneous adipose tissue and fixed (4% PFA in 0.1M phosphate buffer, pH 7.4). Samples were washed with PBS before being incubated with glycine (50mM) and a permeabilisation solution (0.25% saponin, 0.1% BSA in 1x PBS). Adipose tissue axon bundles were then incubated with a blocking solution (0.2% BSA, 5% goat serum, 50 mM NH$_4$Cl, 0.1% saponin, 150 mM NaCl in 20 mM

phosphate buffer) for 20', before incubation with anti-GFP antibody (1:500, A-11122 Invitrogen) for 2h at room temperature. Samples were washed with PBS and incubated with secondary antibody conjugated to 1.4nm gold particles (#2003 Nanogold; Nanoprobes). Nanogold particles were dilated with gold particle amplification solution (GE BEEM; Nanoprobes), according to the manufacturer's instructions. Samples were wrapped with resin (Electron Microscopy Science, USA) and cured at 60°C for 48h. Resin blocks were sectioned using a Leica EM UC7 ultramicrotome, and ultra-thin slices (70-90 nm) were visualised using an FEI Talos 120 kV transmission electron microscope. Images were acquired using a Ceta 16M CMOS sensor camera (FEI, Netherlands).

### Mouse Single cell suspensions

For SPC phenotype, 10wo LepR$^{eYFP}$ mice were given an IP overdose of pentobarbitone and perfused with 1x PBS before scWAT axon bundles, BAT axon bundles and Superior Cervical Ganglia were dissected. Axon bundles were digested for 30' at 37°C (shaking) using 2.5mg/ml collagenase II (C6885, Sigma) and 4000U/ml hyaluronidase IV-S (H3884, Sigma) in Hank's Balanced Salt Solution. Ganglia were digested using 2.5mg/ml collagenase I (C2674, Sigma) for 10' at 37°C (shaking), before being washed with FACS buffer (2% FCS, 0.1% Sodium Azide in 1x PBS) and incubated in 0.25% trypsin (25200072, Thermofisher) for 30' at 37°C (shaking). Axon bundles and ganglia were then mechanically digested using syringes with needles of decreasing size (23G, 25G, 27G) to create a single-cell suspension.

For immune cell phenotyping 10wo $Il33^{fl/fl}$ and SPC$^{\Delta Il33}$ mice were culled using $CO_2$ (unperfused), and spleens and adipose tissues were dissected. Spleens were homogenised through a 70μm filter. Adipose tissues were cut up, before digestion with 2.5mg/ml collagenase II (C6885, Sigma) for 30' at 37°C (shaking).

### Flow cytometry

Single cell suspensions (prepared as above) were incubated with Fc block (553142, BD, 1:250) for 10' at 4°C, followed by live/dead stain (Aqua – L34957, Invitrogen; Near IR – L34975, Invitrogen, Sytox Blue – S34857 Thermofisher, 1:250) for 30' at 4°C. Samples were next stained with surface marker antibodies (CD45-AF700 1:500 103128 Biolegend, CD31-Pacific Blue 1:500 102421 Biolegend, TER119-BUV496 1:500 741079 BD, PDGFRα-APC 1:500 135907 Biolegend, ITGβ4-AF405 1:500 FAB405V Thermofisher, CDH5-PE-Cy7 1:500 138015 Biolegend, CD3e-PE-Cy5 1:250 100309 Biolegend, CD4-BV650 1:250 100545 Biolegend, CD8a-BV785 1:500 100749 Biolegend, CD25-ef450 1:200 48-0251-80 eBioscience, CD11b-ef450 1:500 48-0112-82 Thermofisher, CD64-PE 1:500 139303 Biolegend, Siglec F-BUV395 1:500 740280 BD) for 30' at 4°C. Samples were then fixed using the FOXP3 fix/permeabilisation kit (00-5523-00, eBioscience) as per the manufacturer's instructions; and subsequently incubated with antibodies for intracellular markers or corresponding isotype controls (IL-33-PE 1:200 IC3626P R&D, FOXP3-PE 1:200 12-5773-82 Thermofisher, Isotype-PE 1:200 12-4321-83 Thermofisher) overnight at 4°C. Data was acquired using BD Fortessa X-20 cell analyser and analysed using FlowJo. Isotype controls or negative controls were used to set all gates.

### Mouse SCG LepR+ cell bulk RNA seq

Single cell suspensions were prepared from the Superior Cervical Ganglia as above using 10wo LepR$^{eYFP}$ mice. Live, LepR$^{eYFP+}$ cells were sorted using a FACSAria IIu high-speed cell separator before cDNA libraries were prepared according to the Smart-Seq2 protocol[53] with the following adaptations: addition of 1mg/ml ultrapure BSA to lysis buffer, addition of 20μM template strand exchange nucleotide. cDNA library quality was checked CLS760672, CLS138948) and samples were subjected to paired indexing sequencing (Illumina HiSeq 4000). RNA sequencing data were analysed using Seurat. Bulk RNA-sequencing data can be found using the NCBI's Genome Expression Omnibus using the accession number GSE227493.

### Human ganglia single nuclei RNA-seq

Samples remained on dry ice until prior to nuclei isolation, which was carried out at 4°C. Individual ganglia were placed in gentleMACS C tubes (Miltenyi Biotec) containing 5 mL Miltenyi Nuclei extraction buffer, supplemented with 40 U/μl AmbionTM cloned RNAse Inhibitor (ThermoFisher Scientific). Tissue dissociation was performed using the nuclei isolation programme on the gentleMACS Dissociator (Miltenyi Biotec), followed by a 10-minute incubation on ice. Sample lysate was then subjected to a filter series, passing through 100, 70, 30 and 20μm filters (MACS® SmartStrainers, Miltenyi, pluriStrainer®, Pluriselect). Filter flow-through was centrifuged at 1000 x g for 7 minutes at 4°C. Following centrifugation, supernatant was removed, and the nuclear pellet was resuspended in 2 ml suspension buffer (containing 2% biotin-free BSA and 40 U/μl Ambion cloned RNAse Inhibitor diluted in PBS). Resuspended nuclei were passed through a 20 μm filter (pluriStrainer®, Pluriselect) and centrifuged at 1000 x g for 7 minutes at 4°C, before removal of supernatant resuspension in 200 μl resuspension buffer. 10 μl of the nuclei suspension stained with NucBlue (ThermoFisher Scientific) and counted (CountessTM 3, ThermoFisher Scientific). 20,000 nuclei were loaded in one channel of the Chromium system (10x Genomics). Single Cell 3' v3 chemistry was processed according to the manufacturer's instructions (10x Genomics). Libraries were sequenced using the NovaSeq 6000 platform (Illumina).

Raw sequencing data were processed with Cellranger (v6.0.1, 10x Genomics) count including intronic reads and aligned to the human reference genome GRCh38 v39 (Genome Reference Consortium). Seurat (v5) was used for downstream analysis. Nuclei containing <500 genes or >3000 genes or >1.0 % mitochondrial genes were excluded from analyses. Filtered data contained a total of 10,486 nuclei. After log normalization, principal component analysis (PCA) was used to identify highly variable genes for linear dimension reduction. Unsupervised clustering with a resolution of 1.55 and Uniform Manifold Approximation and Projection (UMAP) were applied for embedding and visualization, followed by the addition of supervised cluster labelling. Density plots showing the

**Immunity**
**Article**

**CellPress**

co-expression of two genes were generated using R package Nebulosa. Single nuclei RNA sequencing data can be found using the NCBI's Genome Expression Omnibus using the accession number GSE241386.

### Published single-cell RNA sequencing analysis

*Lepr* and *Il33* co-expression in the hypothalamus and peripheral organs was assessed using published data[24] (GSE93374) and the *Tabula Muris* database[25] (GSE109774). Gene expression of IL-33+ muscle sensory nerve-associated stromal cells was determined using published data[19] (GSE127005). All data was analysed using Seurat as described.[54]

### RNA extraction, cDNA generation and qPCR

Frozen brown adipose tissue samples were homogenised in TRIzol (PreCellys 24 tissue homogeniser). After the addition of chloroform, the aqueous phase was carefully removed and nucleic acids were precipitated with isopropanol overnight at -20°C. Samples were DNAse treated (B0303s/ M0303s, NEB) and RNA concentrations were measured with the Nanodrop. cDNA was generated using 1000ng of RNA and SuperScript II Reverse Transcriptase (18064-014, Invitrogen) as per the manufacturer's instructions. qPCR was performed with Power SYBR Green Master Mix (4367659, Thermofisher), 20ng of cDNA and primers (*Il1b*F-TGGACCTTCCAGGAT GAGGACA, *Il1b*R-GTTCATCTCGGAGCCTGTAGTG, *iNos*F-GTTCTCAG CCCAACAATACAAGA, *iNos*R-GTGGACGGGTCGATGT CAC, *Tnfa*F-ATGAGCACAGAAAGCATGATC, *Tnfa*R-TACAGGCTTGTCACTCGAATT, *Il6*F-AAAGCCAGAGTCCTTCAGAGAGATAC, *Il6*R-CTGTTAG GAGAGCATTGGAAATTG, *Tbp*F-ACCGTGAATCTTGGCTGTAAAC, *Tbp*R-GCAGCAAATCGCTTGGG ATTA, *Ucp*1F-GTGAAGGTCAGAATGCAAGC, *Ucp1*R-AGGGCCCCCTTCATGAGGTC, *Pgc1a*F-CCCTGCCATTGTTAAGAC, *Pgc1a*R-TGCTGCTG TTCCTGTTTTC, *Elovl3*F-TTCTCACGCGGGTTAAAA ATGG, *Elovl3*R-GAGCAACAGATAGACGACCAC, *Cidea*F-TGCTCTTCTGTATC GCCCAGT, *Cidea*R-GCCGTGTTAAGGAATCTGCTG, *Dio2*F-CAGTGTGGTGCACGTCTCCAATC, *Dio2*R-TGAACCAAAGTT GACCA CCAG, *Pparg*F-TCAAGGGTGCCAGTTTCG, *Pparg*R-GGAGGCCAGCATCGTGT, *Gpr3*F-ATCACCTGAGCAACCGAGAA, *Gpr3*R-AGATGGGGGTGCATTTTACA, *Prdm16*F-CAGCACGGTGAA GCCATT, *Prdm16*R-GCGTGCATCCGCTTGTG, *Lpl*F-CAGCTGGGCC TAACTTTGAG, *Lpl*R-CCTCTCTG CAATCACACGAA). Reactions were run using the BioRad CFX384 well plate reader (50°C: 2'; 95°C: 10'; 40x 95°C: 15s, 60°C: 1') with the addition of a final melt curve. All samples were loaded in technical triplicate. Singular melt curves were confirmed for each condition, and no-template controls were run for each gene to ensure no contamination. An average Ct value was calculated per sample, which was normalised against *Tbp* expression. Normalised expression was presented relative to the appropriate control (=1).

## QUANTIFICATION AND STATISTICAL ANALYSIS

All flow cytometric plots were generated using FlowJo 10.7.1. Confocal images were visualised using Fiji version 2.14.0. Flir Tools was used to blindly quantify BAT and tail temperatures in thermal images. Graphs were plotted and statistical analyses were performed using GraphPad Prism version 9. Data are expressed as Mean +/-SEM. Number of biological samples used per experiment (n), number of individual experiments and statistical tests used for each experiment are included in figure legends. Statistical significance was determined by Student's t test (2 groups) or 2-way ANOVA with post hoc Šidak correction for multiple comparisons. $p < 0.05$ was considered as significant. ns = non-significant, $*p < 0.05$, $**p < 0.01$, $***p < 0.001$, $****p < 0.0001$.